ChemComm

Accepted Manuscript

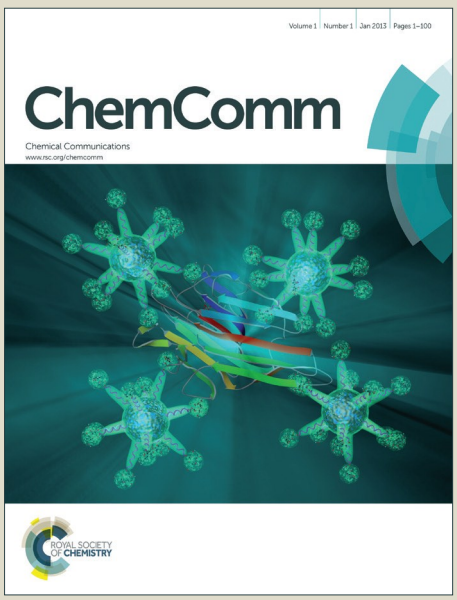

ROYAL SOCIETY OF CHEMISTRY

www.rsc.org/chemcomm

ChemComm

COMMUNICATION

Metal-Metal Chalcogenide Molecular Precursors to Binary, Ternary, and Quaternary Metal Chalcogenide Thin Films for Electronic Devices

Received 00th January 20xx,
Accepted 00th January 20xx

DOI: 10.1039/x0xx00000x

www.rsc.org/

Ruihong Zhang[a], Seonghyuk Cho[b], Daw Gen Lim[a], Xianyi Hu[a], Eric A. Stach[c], Carol A. Handwerker[a], and Rakesh Agrawal[b]

Bulk metals and metal chalcogenides are found to dissolve in primary amine-dithiol solvent mixtures at ambient conditions. Thin-films of CuS, SnS, ZnS, $Cu_2Sn(S_xSe_{1-x})_3$, and $Cu_2ZnSn(S_xSe_{1-x})_4$ (0≤x≤1) were deposited using the as-dissolved solutions. $Cu_2ZnSn(S_xSe_{1-x})_4$ solar cells with efficiencies of 6.84% and 7.02% under AM 1.5 illumination were fabricated from two example solution precursors, respectively.

Metal chalcogenides, such as Cu_2S, Cu_2Se, CuS, CuSe, SnS, SnSe, ZnS, ZnSe, $Cu_2Sn(S_xSe_{1-x})_3$ (0≤x≤1) (CTSSe) and $Cu_2ZnSn(S_xSe_{1-x})_4$ (0≤x≤1) (CZTSSe) have received substantial attention for their applications as photovoltaics,[1-10] optoelectronics,[11,12] piezoelectronics,[13,14] and thermoelectronics.[15-17] Direct solution processing of these semiconductor thin films by roll-to-roll printing on flexible substrates has a great potential to produce low-cost and wearable electronic devices. However, the extremely low solubility of metals and chalcogenide in common solvents, coupled with impurity contamination (*e.g.* O and Cl) derived from elemental sources, have previously slowed down the development of direct solution methods.

To date, the most successful direct solution approach for depositing metal chalogenide thin films is based on hydrazine solutions. Mitzi *et al*. dissolved SnS_2 and In_2Se_3 powders in anhydrous hydrazine, and deposited $SnSe_{2-x}S_x$ and In_2Se_3 as active channels in thin-film transistors.[18,19] Similar methods were successfully applied to CIGSSe[20-22] and CZTSSe thin-film solar cells.[23,24] Unfortunately, using hydrazine creates additional safety and health risks during device processing due to its high toxicity, instability, and carcinogenic properties. In addition, given that zinc and zinc chalcogenides (*e.g.* ZnS and ZnSe) are barely dissolved in hydrazine, a slurry was used for the deposition of CZTSSe thin films.[23] It is therefore of interest to develop a less toxic and more stable solvent system that is highly capable to dissolve a diverse range of materials.

Toward this goal, Webber *et al*. reported that nine V_2VI_3 chalcogenides and tellurium were soluble in a mixture of 1,2-ethylenediamine and 1,2-ethanedithiol.[25-27] Then, Lin *et al.* showed that Cu_2X and In_2X_3 (X=S, Se) are also soluble in the same solvent mixture, and semiconductor alloys, $CuInS_xSe_{1-x}$ (x=0~1), were prepared by annealing combined metal-chalcogenide solutions.[28] However, these studies do not report any device performance based on this ethylenediamine-ethanedithiol solvent mixture. The question that remains to be answered is whether an amine-thiol solvent system is suitable for fabricating thin-film electronic devices.

Here, we demonstrate that a versatile primary amine-dithiol solvent system can readily dissolve not only metal chalcogenides (*e.g.* Cu_2S, Cu_2Se, CuS, CuSe, SnS, SnSe, In_2S_3, In_2Se_3, Ag_2S, and Ag_2Se) but also pure metals (*e.g.* Cu, Zn, Sn, and In) at high concentrations (*e.g.* ≥0.3 M) at room temperature and ambient pressure. The fact that bulk zinc can quickly dissolve in this primary amine-dithiol solvent mixture at high concentrations (>0.75 M) is critical to the deposition of CZTSSe thin films. Given that zinc and zinc chalcogenides (*e.g.* ZnS and ZnSe) are sparingly soluble in most solvents, even in hydrazine, two categories of CZTSSe precursor solutions have been previously reported in the literature to fabricate thin-film solar cells: 1) Hydrazine slurries containing *in-situ* formed ZnX-(N_2H_4) (X=S, Se) particles of a few hundred of nanometers;[23,29] 2) Molecular precursors composed of dissolved metal salts or metal oxides.[30,31] In the former case, the compositional fluctuation within the precursor films is significant due to the presence of those particles, while the latter one introduces possible contamination from other elements like oxygen, chlorine, iodine, etc. The complete dissolution of Zn metal in this primary amine-dithiol solvent system ensures intermixing of precursors on a molecular level and compositional uniformity of deposited CZTSSe thin films. The practicality of this direct solution route is illustrated by depositing CZTSSe

[a] School of Materials Engineering, Purdue University, West Lafayette, IN 47907, USA, E-mail: ruihong.zhang.1@purdue.edu; handwerker@purdue.edu.
[b] School of Chemical Engineering, Purdue University, West Lafayette, IN 47907, USA, Corresponding author: Rakesh Agrawal, E-mail: agrawalr@purdue.edu.
[c] Center for Functional Nanomaterials, Brookhaven National Laboratory, Upton, NY 11973, USA, E-mail: estachbnl@gmail.com.

† Electronic Supplementary Information (ESI) available: including photos of solutions, the electrolytic conductivity measurements on solvents and zinc solutions, TGA results, CZTS film deposition and characterization, CZTSSe film composition analysis, and J-V curves of solar cells. See DOI: 10.1039/x0xx00000x

thin films from metal-metal chalcogenide and metal-chalcogen molecular precursors that give solar cell efficiencies of 6.84% and 7.02%, respectively, in this preliminary work. Besides the quaternary thin films, binary thin films like ZnS, CuS, and SnS, and ternary thin films of CTSSe were successfully deposited from pure metal, metal chalcogenide, or metal-metal chalcogenide precursor solutions, highlighting the potential of this solution route.

Precursor solutions of pure metals (*e.g.* Cu, Zn, Sn, and In) or binary metal chalcogenides (*e.g.* Cu_2S, Cu_2Se, CuS, CuSe, SnS, SnSe, In_2S_3, In_2Se_3, Ag_2S, and Ag_2Se) were readily prepared by dissolving bulk powders in solvent mixtures of primary amine (*e.g.* butylamine (BA), hexylamine (HA), etc.) and 1,2-ethanedithiol (EDT) at ambient conditions (Table S1). Fig. 1a and Fig. S1 shows the solutions prepared after the complete dissolution of above bulk powders in HA-EDT solvent mixtures (vol. ratio 1:1). Note that neither HA/BA nor EDT alone

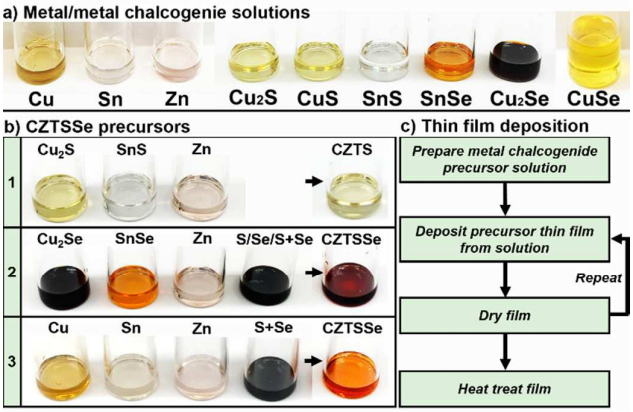

Fig.1 a) Solutions prepared by dissolving Cu, Sn, Zn, Cu_2S, CuS, SnS, SnSe, Cu_2Se, and CuSe in solvent mixtures of HA-EDT (vol ratio. 1:1, conc. 0.3 M) at ambient temperature and pressure. b) Three types of combined precursors and constituent solutions. c) Schematic of general deposition procedures.

dissolves metals or metal chalcogenides. As soon as EDT was added into the mixture of amine and powders at room temperature, the dissolution started immediately, and vice versa. Solubility limits of Cu, Zn, Sn, Cu_2S, Cu_2Se, SnS, and SnSe in BA-EDT (vol. ratio 1:1) at 25°C are around 0.5, 0.78, 0.3, 0.5, 0.3, and 0.3 mol/L, respectively. All precursor solutions stay optically transparent over months after complete dissolution, indicating the formation of stable organometallic complexes.

To qualitatively understand why bulk metals dissolve in these primary amine-dithiol solvent mixtures, electrolytic conductivity measurements were performed on BA, HA, EDT, HA-EDT solvent mixture, BA-EDT solvent mixture, and solutions with incremental amounts of dissolved Zn metals at 25°C (Table S2). Although BA, HA, and EDT showed zero conductivity, conductivities of 1926.5 µS/cm and 550.2 µS/cm are exhibited by solvent mixtures of BA-EDT (vol. ratio 1:1) and HA-EDT (vol. ratio 1:1), respectively. Furthermore, an inverse relationship between the Zn concentration and the solution conductivity has been observed. The changes in conductivities indicate charged species are formed as soon as BA/HA and EDT are mixed, and the formation of metal complexes consume some of charged species. It is highly possible that deprotonated thiols and protonated amines are generated in the solvent mixture. The deprontonated thiols and metal ions then formed complexes while the bulk metal was dissolving. The complexes formed are expected to have the similar structure as zinc ethane-1,2-dithiolato complex, $[Zn(edt)_2]^{2-}$ reported by Rao *et al.*[32] The as-dried and as-annealed films of a Zn solution were characterized using grazing incident X-ray diffraction (GIXRD) (Fig. S2). After annealing at 300°C, the amorphous precursor film converted to ZnS, which was composed of zincblend (F-43m) and wurtzite ZnS ($P6_3m$) phases. This indicates that EDT acts as a sulfur source for the conversion of a metal into its corresponding metal sulfide.

The re-deposition of metal chalcogenide solutions enables rapid fabrication of a variety of semiconductor thin films. Herein, we show the re-deposition of CuS and SnS solutions as examples. Fig. 2a and 2b show the GIXRD pattern and Raman spectrum of a thin film deposited from CuS solution and subsequently annealed at 300°C. All the XRD peaks match those in the standard CuS pattern (space group *$P6_3/mmc$*, JCPDS 06-0464). The Raman shifts exhibit peaks at 266 cm^{-1} and 474 cm^{-1} corresponding to covellite CuS reported by Sukarova *et al.*[33] In the case of SnS re-deposition, thermogravimetric analysis (TGA) shows an end point of phase transformation at 300°C (Fig. S3). The orthorhombic SnS is the only phase formed after annealing at 300°C, as shown in GIXRD pattern and Raman spectrum (Fig. 2c and 2d). The Raman peaks at 83, 95, 163, 191, 219, and 288 cm^{-1} match well with those from a single crystal SnS (85, 95, 164, 192, 218, and 290 cm^{-1}).[34] The above examples illustrated that metal chalcogenides thin films can be recovered from the precursor solutions through efficient deposition technique and well-controlled annealing process.

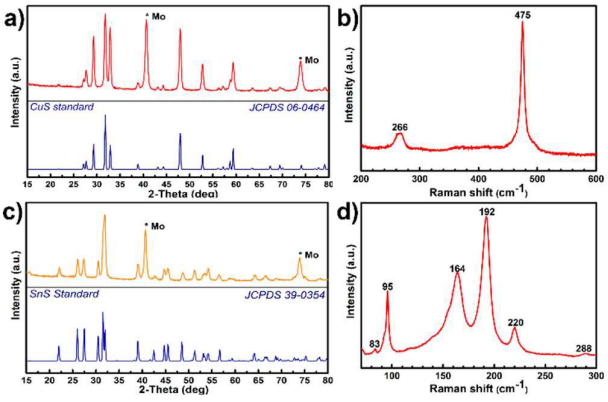

Fig.2 GIXRD patterns and Raman spectra of thin films deposited from CuS and SnS solutions and subsequently annealed at 300°C. a) and b) CuS, c) and d) SnS.

Owing to the versatility of this primary amine-dithiol solvent mixture in dissolving multiple metal and chalcogen sources at high concentrations, a universal pathway is provided to design molecular precursors for depositing specific metal chalcogenides, especially for ternary and quaternary compounds with tunable bandgaps. To make precursors for ternary $Cu_2Sn(S_xSe_{1-x})_3$ ($0 \le x \le 1$), solutions of Cu_2S/Cu_2Se,

SnS/SnSe, and S/Se are mixed with proper ratios. The flexibility in adjusting S:Se ratios in the precursor solutions allows the fabrication of ternary sulfide, selenide, and sulfoselenide. The GIXRD patterns and film morphology of ternary $Cu_2Sn(S_xSe_{1-x})_3$ ($0 \le x \le 1$) are shown in Fig. 3.

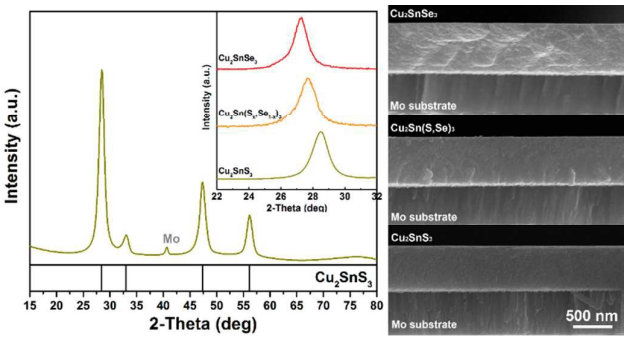

Fig. 3 GIXRD patterns and film morphology of ternary $Cu_2Sn(S_xSe_{1-x})_3$ ($0 \le x \le 1$) thin films processed using mixture solutions of Cu_2S/Cu_2Se, SnS/SnSe, and S/Se. The compositions of the thin films are estimated using SEM-EDX. The standard pattern of Cu_2SnS_3 (PDF 01-070-6338) is labelled at the bottom. Based on Vegard's law,[36] x=0.35 in the $Cu_2Sn(S_xSe_{1-x})_3$ thin film.

To process compositional uniform $Cu_2SnZn(S_xSe_{1-x})_4$ ($0 \le x \le 1$) thin films, three types of CZTSSe precursor solutions have been explored, that is, *Solution 1*: CZTS precursor, a mixture of Cu_2S, SnS, and Zn solutions; *Solution 2*: CZTSSe precursor, a mixture of Cu_2Se, SnSe, Zn, S, and Se solutions; and *Solution 3*: CZTSSe precursor, a mixture of Cu, Sn, Zn, S, and Se solutions (Fig. 1b). The CZTS and CZTSSe films deposited from *Solution 1* and *Solution 3* are described in Fig. S4 and Fig. S7. The use of combined solutions in device fabrication will be illustrated in detail using *Solution 2:CZTSSe precursor* as an example. In *Solution 2*, [Sn]=0.1 M, [Cu]:[Zn]:[Sn]:[S]:[Se]= 1.45:1.05:1:2:2. The deposition of precursor films includes spin coating, solvent drying/annealing, and a final heat treatment process (Fig. 1c). Typically, eight to ten coatings were performed for solar cell fabrication. A kesterite CZTSSe precursor film was formed after annealing coated *Solution 2* at 300°C, as shown in Fig. 4a and 4b. After selenization, Se substituted more S sites in the crystal lattice, indicated by the intense peak at 197 cm^{-1} (A1 mode of CZTSe) in contrast to the peak at 329 cm^{-1} (A1 mode of CZTS) in Raman spectrum (Fig. 4b). No secondary phases were detected by GIXRD or Raman with excitation wavelength of 633 nm. The thin-film solar cells fabricated based on this direct solution route has the highest power conversion efficiency (PCE) of 6.84% (7.04%) for a total area of 0.471 cm^2 (an active area of 0.457 cm^2) (Fig. 4c). Other characteristic parameters of this solar cell are: J_{sc} of 35.5 $mA \cdot cm^{-2}$, V_{oc} of 0.36 V, and fill factor (FF) of 53.5%. The bandgap of the absorber layer is estimated to be 1.08 eV based on external quantum efficiency (EQE) measurement (Fig. 4d).

The composition and microstructure of the precursor film and the selenized film were characterized using scanning electron microscopy (SEM) and scanning transmission electron microscopy (STEM) equipped with energy-dispersive X-ray spectroscopy (EDX). Fig. S5 and Table S3 illustrates the SEM-EDX results of the precursor film and the selenized film. High-angle annular dark field (HAADF) images in Fig. 5a shows that the precursor film consists of multiple layers which were created by spin coating. The high- and low-contrast regions are attributed to the *in-situ* formed nanoparticles and low-mass residual solutions. The *in-situ* formed nanoparticles are less than 5 nm with a narrow size distribution (Fig. S6). Fig. 5b shows the elemental distributions within a precursor layer and across precursor layers. The compositional fluctuation of this precursor film is much smaller compared to that of the hydrazine-slurry processed precursor film.[24] Fig. 5c and 5d are the cross-sectional STEM images and compositional linescan of a processed solar cell. In the absorber layer, a fine-grained layer formed underneath the large-grained layer after selenization (Fig. 5c). The concentrations of Cu, Zn, Sn, S, and Se are uniform in the large-grained layer, while the concentrations of Cu and Zn have some fluctuations in the fine-grained layer. The S:Se ratio is believed to have played an important role in changing the grain growth behavior during selenization as reported by colloidal routes studies,[5,36] leading to the formation of a fine-grained layer in this case.

Solar cells of CZTSSe were also successfully processed from *Solution 3* which is composed of solutions of Cu, Zn, Sn, S, and Se. Our preliminary study shows a PCE of 7.02% on a total area of 0.4862 cm^2 without an anti-reflection coating (Fig. S7). The efficiencies are believed to be improved by increasing the absorber thicknesses.

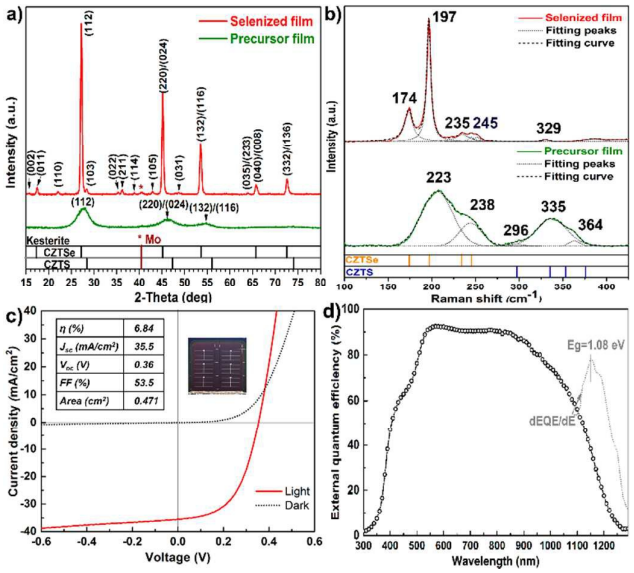

Fig. 4 Results for thin-film solar cells processed from *Solution 2*: CZTSSe precursor. a) GIXRD patterns and b) Raman spectra of the precursor and the selenized film. c) J-V curves and performance parameters for the best performing cell in the dark and under AM1.5 illumination. The inset is the final device. d) EQE measurement.

In conclusion, a primary amine-dithiol solvent system is used for rapid dissolution of bulk metals (*e.g.* Cu, Zn, Sn, and In) and metal chalcogenides (*e.g.* Cu_2S, Cu_2Se, CuS, CuSe, SnS, SnSe, In_2S_3, In_2Se_3, Ag_2S, and Ag_2Se). The extensive applications of solution routes based on this versatile solvent system is demonstrated by film deposition of CuS, SnS, ZnS, CTSSe, CZTS, and CZTSSe. The unique capability to dissolve Zn powders at room temperature allows the formation of molecular

precursors for CZTSSe deposition, and promotes the phase purity and compositional uniformity in the final films. Furthermore, the use of the metal-metal chalcogenide precursor solutions offers flexibility in tailoring the stoichiometry of the resulting films simply by adjusting the types and concentrations of the incorporated component solutions. Preliminary results of the solar cell performances illustrate the potential of this direct solution route for photovoltaic device and other electronic applications. We expect that the efficiencies will improve after further refinement in film compositions and heat treatment conditions.

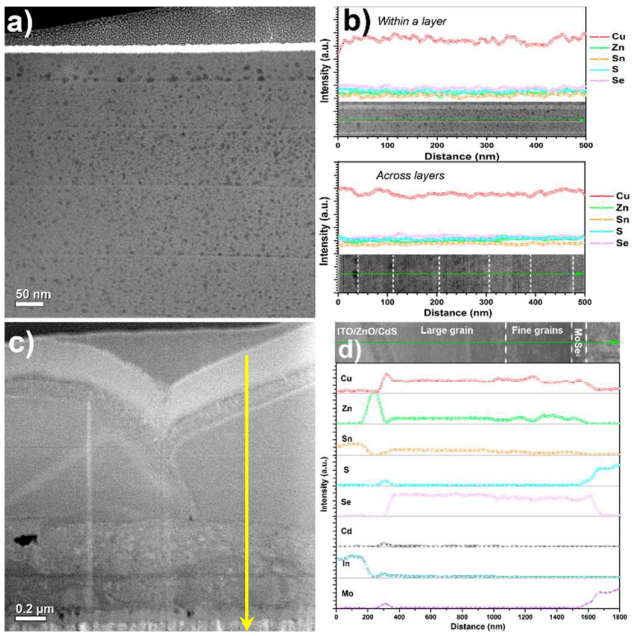

Fig. 5 Results for *Solution 2*: CZTSSe precursor. a) STEM-HAADF images of CZTSSe precursor film. b) STEM-EDX compositional profiling of Cu, Zn, Sn, S, and Se within a single layer of precursor film and across several precursor films. c) Cross-sectional STEM-HAADF image of a processed solar cell. d) STEM-EDX compositional profiling show the distribution of elements in this device. Note that X-rays of S $K^{\alpha 1}$ and Mo $L^{\alpha 1}$ overlap each other, and thus the compositional profiles are the same.

The authors acknowledge C. K. Miskin, R. Boyne, P. Murria, L. Cain and Professor H. Kenttamaa, for assisting in the solution analysis. The authors also want to thank M. Koeper for performing quantum efficiency measurement, K. Brew and B. Graeser for preparing Mo-coated soda lime glass. This research was funded by NSF Solar Economy IGERT program (0903670-DGE).

References

1. J. A. Bragagnolo, A. M. Barnett, J. E. Phillips, R. B. Hall, A. Rothwarf and J. D. Meakin, *Electron Devices, IEEE Transactions on*, 1980, **27**, 645.
2. S. C. Riha, B. A. Parkinson and A. L. Prieto, *Journal of the American Chemical Society*, 2009, **131**, 12054.
3. Q. Guo, G. M. Ford, W.-C. Yang, B. C. Walker, E. A. Stach, H. W. Hillhouse and R. Agrawal, *J Am Chem Soc*, 2010, **132**, 17384.
4. S. C. Riha, B. A. Parkinson and A. L. Prieto, *Journal of the American Chemical Society*, 2011, **133**, 15272.
5. C. K. Miskin, W.-C. Yang, C. J. Hages, N. J. Carter, C. S. Joglekar, E. A. Stach and R. Agrawal, Progress in Photovoltaics: Research and Applications, **2015**, 23, 654
6. H. Okimura, T. Matsumae and R. Makabe, *Thin Solid Films*, 1980, **71**, 53.
7. K. T. Ramakrishna Reddy, N. Koteswara Reddy and R. W. Miles, *Solar Energy Materials and Solar Cells*, 2006, **90**, 3041.
8. P. Sinsermsuksakul, K. Hartman, S. Bok Kim, J. Heo, L. Sun, H. Hejin Park, R. Chakraborty, T. Buonassisi and R. G. Gordon, *Appl Phys Lett*, 2013, **102**, 053901.
9. C. Steinhagen, M. G. Panthani, V. Akhavan, B. Goodfellow, B. Koo and B. A. Korgel, *Journal of the American Chemical Society*, 2009, **131**, 12554.
10. J. Tang, Z. Huo, S. Brittman, H. Gao and P. Yang, *Nat Nano*, 2011, **6**, 568.
11. J. Lim, M. Park, W. K. Bae, D. Lee, S. Lee, C. Lee and K. Char, *Acs Nano*, 2013, **7**, 9019.
12. H. Shen, X. Bai, A. Wang, H. Wang, L. Qian, Y. Yang, A. Titov, J. Hyvonen, Y. Zheng and L. S. Li, *Adv Funct Mater*, 2014, **24**, 2367.
13. M. Catti, Y. Noel and R. Dovesi, *J Phys Chem Solids*, 2003, **64**, 2183-2190.
14. M.-Y. Lu, J. Song, M.-P. Lu, C.-Y. Lee, L.-J. Chen and Z. L. Wang, *Acs Nano*, 2009, **3**, 357.
15. H. Liu, X. Shi, F. Xu, L. Zhang, W. Zhang, L. Chen, Q. Li, C. Uher, T. Day and G. J. Snyder, *Nat Mater*, 2012, **11**, 422.
16. S. Sassi, C. Candolfi, J.-B. Vaney, V. Ohorodniichuk, P. Masschelein, A. Dauscher and B. Lenoir, *Appl Phys Lett*, 2014, **104**, 212105.
17. L.-D. Zhao, S.-H. Lo, Y. Zhang, H. Sun, G. Tan, C. Uher, C. Wolverton, V. P. Dravid and M. G. Kanatzidis, *Nature*, 2014, **508**, 373.
18. D. B. Mitzi, *J Mater Chem*, 2004, **14**, 2355.
19. D. B. Mitzi, *Adv Mater*, 2009, **21**, 3141.
20. D. B. Mitzi, T. K. Todorov, O. Gunawan, Y. Min, C. Qing, L. Wei, K. B. Reuter, M. Kuwahara, K. Misumi, A. J. Kellock, S. J. Chey, T. G. de Monsabert, A. Prabhakar, V. Deline and K. E. Fogel, 2010.
21. D. B. Mitzi, M. Yuan, W. Liu, A. J. Kellock, S. J. Chey, V. Deline and A. G. Schrott, *Adv Mater*, 2008, **20**, 3657.
22. T. K. Todorov, O. Gunawan, T. Gokmen and D. B. Mitzi, *Prog Photovoltaics*, 2013, **21**, 82.
23. T. K. Todorov, K. B. Reuter and D. B. Mitzi, *Adv Mater*, 2010, **22**, E156-+.
24. T. K. Todorov, J. Tang, S. Bag, O. Gunawan, T. Gokmen, Y. Zhu and D. B. Mitzi, *Adv Energy Mater*, 2013, **3**, 34.
25. P. D. Antunez, D. A. Torelli, F. Yang, F. A. Rabuffetti, N. S. Lewis and R. L. Brutchey, *Chem Mater*, 2014, **26**, 5444.
26. D. H. Webber and R. L. Brutchey, *Journal of the American Chemical Society*, 2013, **135**, 15722.
27. D. H. Webber, J. J. Buckley, P. D. Antunez and R. L. Brutchey, *Chemical Science*, 2014, **5**, 2498.
29. Z. Lin, Q. He, A. Yin, Y. Xu, C. Wang, M. Ding, H.-C. Cheng, B. Papandrea, Y. Huang and X. Duan, *Acs Nano*, 2015, **9**, 4398.
28. T. Todorov, H. Sugimoto, O. Gunawan, T. Gokmen and D. B. Mitzi, *Ieee J Photovolt*, 2014, **4**, 483.
30. Q. Tian, G. Wang, W. Zhao, Y. Chen, Y. Yang, L. Huang and D. Pan, *Chem Mater*, 2014, **26**, 3098.
31. R. Zhang, S. M. Szczepaniak, N. J. Carter, C. A. Handwerker and R. Agrawal, *Chem Mater*, 2015, **27**, 2114-2120.
32. C. P. Rao, J. Dorfman and R. Holm, *Inorg Chem*, 1986, **25**, 428.
33. B. Minceva-Sukarova, M. Najdoski, I. Grozdanov and C. Chunnilall, *Journal of molecular structure*, 1997, **410**, 267.
34. H. Chandrasekhar, R. Humphreys, U. Zwick and M. Cardona, *Phys Rev B*, 1977, **15**, 2177.
35. A. R. Denton and N. W. Ashcroft, *Physical Review A*, 1991, **43**, 3161.
36. B. C. Walker, B. G. Negash, S. M. Szczepaniak, K. W. Brew and R. Agrawal, *Photovoltaic Specialists Conference (PVSC)*, 2013, IEEE **39**, 2548.